Effect of the countermaterial on the tribological behavior of $Cu_{45}Zr_{46}Al_7Nb_2$ Bulk Metallic Glass

Solène BARLEMONT[1], Guillaume COLAS[1], Alexis LENAIN[2], Pierre-Henri CORNUAULT[1]*

[1] Univ. Bourgogne Franche-Comté FEMTO-ST Institute CNRS/UFC/ENSMM/UTBM,
Département de Mécanique Appliquée, Besançon, 25000, France
solene.stoens@femto-st.fr ; guillaume.colas@femto-st.fr ; pierre-henri.cornuault@ens2m.fr

[2] Vulkam Inc. Amorphous metal micro casting / www.vulkam.com / Gières, 38610, France
alexis.lenain@vulkam.com

* Corresponding author:
Pierre-Henri CORNUAULT
E-mail: pierre-henri.cornuault@ens2m.fr
Femto-ST Institute – Département de Mécanique Appliquée
24, rue de l'épitaphe
25000 Besançon
France

Abstract Reference Number

Abstract

Bulk Metallic glasses (BMGs) are produced through an extremely fast cooling process of a liquid metallic alloy (with a specific composition), so that the final solid state material is deprived of crystalline structure. The resulting mechanical properties of BMGs are of great interest for number of applications, including tribological applications. Recent studies highlighted a probable dependence of the friction and wear of BMGs on the counterface material. The present study investigates the relationship between the tribological behavior of $Cu_{45}Zr_{46}Al_7Nb_2$ BMG plates and six different countermaterials under linear reciprocating sliding. The selected countermaterials are: AISI 52100 and AISI 440C steels, brass and bronze, $Cu_{45}Zr_{46}Al_7Nb_2$ and $Zr_{60}Cu_{28}Al_{12}$ BMGs. Results confirm that friction and wear are strongly correlated with the creation of a third body in the contact, whose nature (composition and morphology) depends on the countermaterial. Material transfer occurs either from the counterpart to the BMG or vice-versa, and the phenomenon is rather driven by the chemical affinities between the oxides formed than by the hardness and class of countermaterials (*i.e.* steels, Cu-based alloys, and BMGs). BMG/Brass contact indeed exhibits the lowest friction and the lowest wear while friction of BMG/bronze is two-fold higher and wear is among the highest of all the contact configurations tested.

Keywords

Bulk Metallic Glasses, countermaterial, third body, tribochemistry, surface analysis

1 Introduction

Bulk Metallic Glasses (BMGs) are known to demonstrate a combination of excellent mechanical properties (including high yield stress, high elastic strain and high toughness), high corrosion resistance and very low shrinkage due to the lack of crystallization. BMGs have great potential in various engineering applications among which micro-devices involved in contact applications: biomedical applications such as cardiovascular stent and protheses [1], micro and macro devices involved for example in microcantilever sensors and microgears [2]. Tribological behavior of BMGs is thus of primary interest to ensure reliable industrial performance.

However, contact applications imply various counterpart materials. Two recent macroscale studies on the friction of different Cu-Zr, Zr, and Ni based BMGs sliding against AISI 52100 balls raised the question of the role of the counterpart and the surrounding environment [3,4]. The studies eventually suggest that counterpart composition and the surrounding environment both have greater influence than the BMG composition itself. At the microscale, Caron *et al* [5] also highlighted the dependence of friction on the chemical composition of the counter body in a wearless regime during sliding tests conducted through atomic and friction force microscopy (AFM and FFM).

To the best of our knowledge, only Zhong *et al* [6] provide a direct comparison of several counterfaces in contact with a BMG during friction tests. Friction tests were carried out between $Zr_{41}Ti_{14}Cu_{12.5}Ni_{10}Be_{22.5}$ pins and discs made of AISI 5120, AISI 51200, and $Zr_{41}Ti_{14}Cu_{12.5}Ni_{10}Be_{22.5}$ on a pin-on-disc tribometer under heavy loads. The smallest friction coefficient is 0.2 and is obtained with the BMG counterface. In this BMG/BMG configuration, the pin is more wear resistant than the plate, although in the BMG/steel configurations, the BMG pin suffers from higher wear than the steel disks. Unfortunately, no chemical analyses of the friction track have been performed in order to identify the nature of material transfer, although such a third body layer seems to play a key role in the wear mechanisms. Finally, the normal loads of 100 to 150 N that are applied on the pins of 4 mm in diameter induces contact pressures ranging from 8 to 12 MPa. These particularly low pressures might induce completely different wear mechanisms compared to the significantly higher contact pressures involved in the above-mentioned applications.

In the literature, most studies focus on the tribological behavior of BMGs against a unique counterpart. The selected counterpart belongs either to steels and stainless steels (AISI 52100 [7–10], AISI 8660 [11], GCr6 [12], GCr15 [13], AISI 304 [14], and AISI 303 [15]), or to hard ceramics (SiC [16], Zirconia [15], Si_3N_4 [17,18], and WC [19–21]). Material transfer is often observed with metallic counterfaces, while the use of harder ceramic counterfaces mainly results in micro-cracking and plastic deformation of the BMG. However, no direct comparison between the above-mentioned studies can be made due to the diversity of contact conditions (contact geometry, contact pressure, sliding speed, environment).

The present study aims at studying the tribological behavior of $Cu_{45}Zr_{46}Al_7Nb_2$ BMG against different counterpart materials under identical contact conditions, in order to determine the impact of the countermaterial on the tribological behavior.

2 Materials and methods

The selected composition of BMG is $Cu_{45}Zr_{46}Al_7Nb_2$. It combines the advantages of Cu-Zr-based BMGs of both high glass forming ability (GFA) and high mechanical properties. Samples were processed by arc-melting bulk fragments of each elements of high purity (> 99.9 %) under argon atmosphere. The primary alloys were melted at least five times and then were injected into molds to

produce plate-shaped samples (15×10×1 mm^3). Samples were then polished with sandpaper and ultrasonically cleaned during 3 min at 70°C in isopropyl-alcohol before being dried in air. The Sa roughness parameter of the polished samples is close to 70 nm and was measured using a variable focus optical microscope (InfiniteFocus, Alicona Imaging GmbH). Cu$_{45}$Zr$_{46}$Al$_7$Nb$_2$ BMG plates will be named CuZr plates throughout this paper for the sake of clarity.

Friction tests were performed using an in-house designed ball-on-plate tribometer. Six different counterpart materials were selected for the present study. They could be divided into three categories. The first "steels" category includes AISI 52100 and AISI 440C balls of 5 mm diameter. The second "Cu-based alloys" category includes brass and bronze balls of 5 mm diameter. The last category is made up of two BMGs, among which a composition identical to the plate sample (Cu$_{45}$Zr$_{46}$Al$_7$Nb$_2$) and a Zr-rich composition (Zr$_{60}$Cu$_{28}$Al$_{12}$), named CuZr roller and Zr roller respectively. Because the as-cast BMG samples were 1 mm thick, they were machined into rollers of 5 mm diameter with a 2.5 mm curvature radius in the transverse direction, so that the contact geometry was identical to that of the 5 mm diameter balls. The Vickers hardness of each material was measured with a load of 10 kg and 5 measurements were performed to ensure meaningful average calculation. The naming, geometry, chemical composition, and hardness of both the CuZr plate and counterfaces are listed in Table 1.

Table 1 – Naming, geometry, chemical composition and hardness of the studied samples. The "roller" and "ball" geometries refer to the counterparts.

Sample naming	Sample geometry	Material	Composition (wt%)	Hardness (HV)
CuZr plate	Plate	Cu$_{45}$Zr$_{46}$Al$_7$Nb$_2$ BMG	Cu 37%, Zr 54%, Al 2%, Nb 7%	477 ± 12
CuZr roller	Roller			
Zr roller	Roller	Zr$_{60}$Cu$_{28}$Al$_{12}$ BMG	Cu 23%, Zr 72%, Al 5%	434 ± 6
440C	Ball	AISI 440C stainless steel	Fe 81%, Cr 16%, C 1%, Mo 0.48%, Mn 0.38%, Si 0.34%, Ni 0.12%, P 0.03%	740 ± 10
52100	Ball	AISI 52100 steel	Fe 97%, Cr 1.4%, C 1%, Mn 0.38%, Si 0.26%, P 0.01%	824 ± 12
Brass	Ball	CuZn38 brass	Cu 61%, Zn 38%, Fe 0.02%, Pb 0.01%	192 ± 3
Bronze	Ball	Bronze	Cu 93%, Sn 6.5%, P 0.2%, Pb 0.01%	221 ± 10

Friction tests were carried out under reciprocating linear motion with a ± 1 mm displacement stroke at 1 Hz, which corresponds to a sliding speed of 4 mm/s. Tests were conducted at least three times under identical configuration to assess results reproducibility. A constant normal force (F_N) of 1 N was applied using dead weight during a total test duration of 5,000 backward-and-forward friction cycles. Tests were performed in ambient air, and the relative humidity was maintained at 50 ± 2 %RH using a set up with an external flask of NaOH solution as described in a previous work [3]. Throughout each test, the relative displacement of the ball (h) and the friction force (F_T) were measured thanks to a LVDT sensor and a piezoelectric sensor, respectively. For each friction cycle, an average friction coefficient μ was calculated from an energetic point of view using (1), where Δh_0 is the distance between the two extremities of the friction track where $F_T = 0$. For each test, a stabilized friction coefficient μ_{stab} is then calculated according to (2). μ_{stab} corresponds to the mean of all μ values of the steady state friction, namely between 3,000 to 5,000 cycles.

$$\mu = \frac{1}{2\Delta h_0} \int \frac{|F_T|}{F_N}\, dh \qquad (1)$$

$$\mu_{stab} = \frac{1}{2,000} \sum_{i=3,000}^{5,000} \mu_i \qquad (2)$$

After friction test, surface topography characterization of each friction tracks (balls and plates) was performed using a variable focus optical microscope (InfiniteFocus, Alicona Imaging GmbH). The three-dimensional surface topographies were then analyzed using the software Gwyddion in order to calculate wear volumes, according to the method described by Ayerdi *et al* [22]. In this study, wear was defined as a loss of material volume, which means that material transfer can lead to negative wear as opposed to material detachment which leads to positive wear. The wear rates K ($mm^3.N^{-1}.m^{-1}$) of the plate (K_{plate}) and of the ball (K_{ball}) were defined as the wear volume normalized by units of sliding distance and normal force, as described in (3). V_{plate} and V_{ball} are the wear volumes of the plate and the ball respectively (mm^3), $2 \times \Delta h_0$ is the distance covered in one cycle, N_c is the number of cycles, and F_N is the normal force applied (N).

$$K_{plate} \text{ (or } K_{ball}) = \frac{V_{plate} \text{ (or } V_{ball})}{2 \times \Delta h_0 \times N_C \times F_N} \qquad (3)$$

Friction track morphology and chemical elemental composition were studied by Scanning Electron Microscopy (SEM) and Energy Dispersive Spectroscopy (EDS). SEM observations were performed using a FEI Apreo SEM, equipped with backscattered electrons detector (BSE). The electron beam voltage and current were 5 keV and 0.1 nA respectively. EDS analyses were conducted at 10 keV with a Bruker SD Detector.

3 Results

3.1 Friction and wear behavior

The friction coefficients from the tests performed on the CuZr plates with six different counterparts are displayed on Figure 1. Surprisingly, friction cannot be categorized according to obvious countermaterial groups (steel counterfaces and Cu-based-alloy counterfaces). Four counterfaces, respectively 440C, bronze, CuZr and Zr, can be clustered together in terms of friction level in the steady-state regime, with a μ_{stab} close to 0.5. 52100 is the counterface with the highest μ_{stab}, that reaches 0.66. The μ_{stab} of brass ball against CuZr plate is exceptionally low for a dry sliding configuration, ranging from 0.14 to 0.32, and μ shows outstanding low variations against time. 52100, Bronze, CuZr and Zr stabilize rather quickly between 500 and 800 cycles. Brass is the fastest to reach steady state regime within the first 200 cycles, while it takes 3000 cycles for 440C. Brass is the single counterface that induces a standard deviation of μ_{stab} greater than 0.04. Indeed, the μ_{stab} of one test (displayed in blue on Figure 1) is almost twice as high as the other two. The three curves performed under identical conditions for each counterface highlight a high repeatability of μ during both the running-in process and the steady-state regime, particularly in the cases of friction with 440C, 52100, bronze, CuZr and Zr. The friction behavior of the CuZr plate with the two BMG-counterfaces is indeed significantly similar.
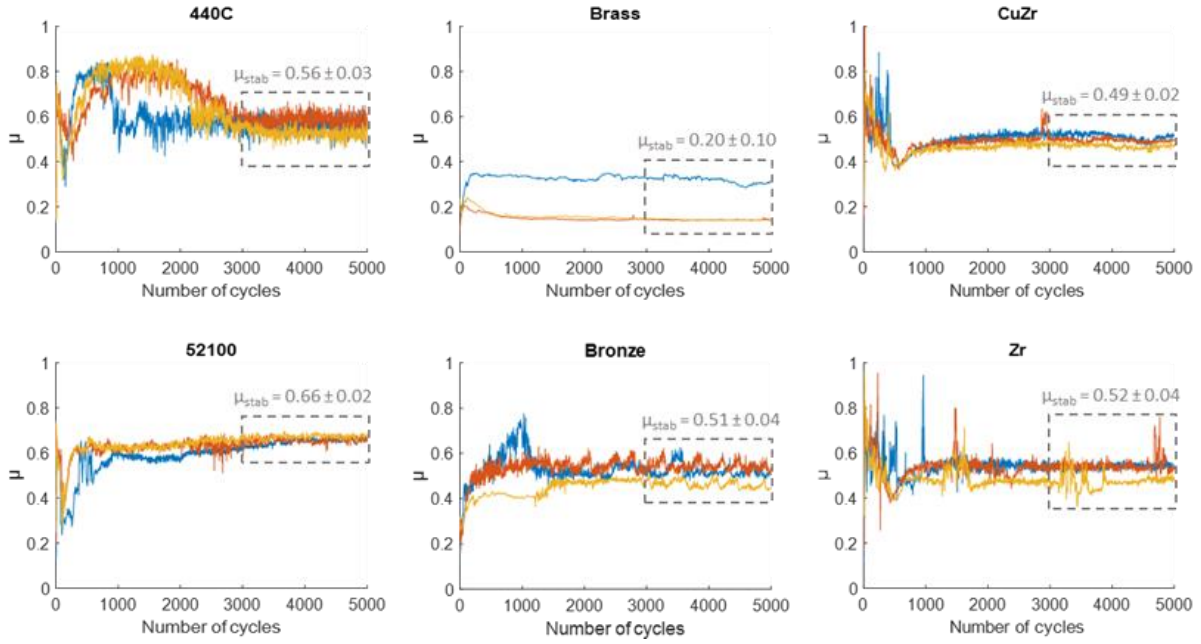
Figure 1 – Evolution of µ versus the number of cycles during friction tests performed on $Cu_{45}Zr_{46}Al_7Nb_2$ with six counterpart materials (440C balls, 52100 balls, brass balls, bronze balls, CuZr and Zr rollers). Three tests performed under identical conditions ($F_N = 1 N$, $v = 4 mm/s$, and RH = 50 ± 2 %) are illustrated by the blue, yellow and red curves.

Figure 2 displays μ_{stab} versus the wear rates of the CuZr plate (K_{plate}) and versus the wear rates of the counterfaces (K_{ball}) for each counterpart material. The values of wear rates (K_{plate} and K_{ball}) are consistent with the three categories of counterfaces previously mentioned:

- CuZr plate against 52100 ball is characterized by K_{plate} close to zero and K_{ball} close to 7×10^{-5} mm^3/Nm (see the green dashed circles on Figure 2).
- CuZr plate against brass ball is characterized by both K_{plate} and K_{ball} close to zero (see the blue dotted circles on Figure 2).
- CuZr plate against 440C, bronze, CuZr and Zr counterparts are all defined by K_{plate} ranging from 5×10^{-5} to 12×10^{-5} mm^3/Nm and K_{ball} ranging from 1×10^{-5} to 5×10^{-5} mm^3/Nm (see the orange dash-dotted circles on Figure 2).

The total wear (the sum of K_{plate} and K_{ball}) is roughly similar between the contacts of CuZr against 440C, 52100, bronze and CuZr. Zr exhibits the highest total wear, while brass demonstrates extremely low total wear. However, the balance of wear between the CuZr plate and the counterface differs (Figure 2). On the one hand, in case of 440C, bronze, CuZr and Zr, the wear rate of the CuZr plate is the largest. On the other hand, the wear rate of the ball is the largest in case of 52100. However, the case of brass is dissimilar. During friction tests between the pair CuZr plate / brass ball, both wear rates of the BMG plate and of the brass ball are close to zero, and wear rates are highly reproducible from one test to another. Indeed, it must be emphasized that the standard deviation of the wear rates related to brass are extremely low compared to other counterfaces, despite the twice as high μ_{stab} of one friction test compared to the other two (Figure 1). This exceptional combination of low friction and high wear resistance of $Cu_{45}Zr_{46}Al_7Nb_2$ against brass predicts very promising behavior for industrial applications. In the case of BMG against BMG, both Zr and CuZr rollers undergo a wear rate close to 3.5×10^{-5} mm^3/Nm. However, the wear rate of the CuZr plate is almost twice as high when rubbing with the Zr roller than with the CuZr roller.
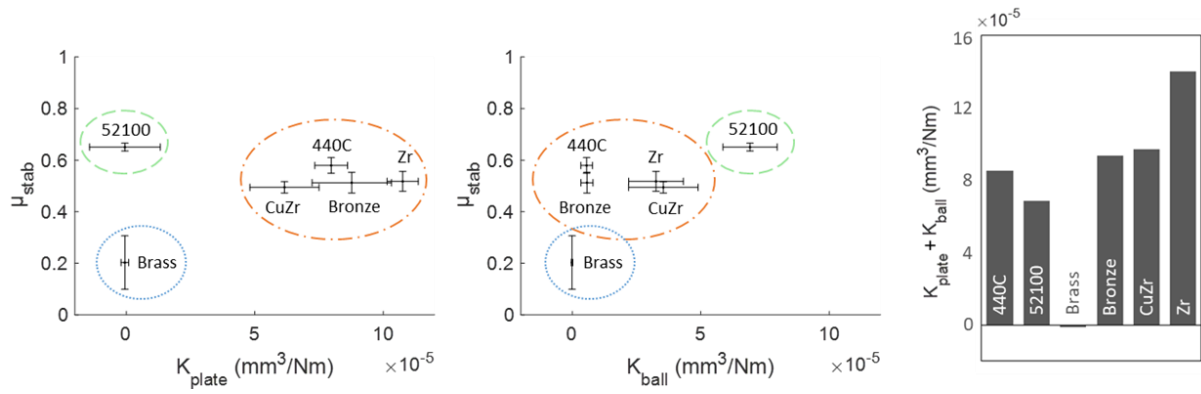
Figure 2 – μ_{stab} versus wear rates of the plates (K_{plate}) and wear rates of the counterfaces (K_{ball}) (left). The dotted colored circles refer to the categories of tribological behavior described in the text. Bar graph of the total wear rate ($K_{plate} + K_{ball}$) for each counterfaces (right).

3.2 Analyses of the worn surfaces

Figure 3 – SEM images of the wear tracks of the plates and of the balls/rollers, for each counterpart materials. Bar plots on the right are elemental composition obtained from EDS analyses performed at points 1 to 5, that correspond for each counterparts to the unworn surface of the plate, the 3ʳᵈ body of the plate scar, the unworn surface of the ball, the 3ʳᵈ body of the ball scar, and the ejected particles around the wear track of the ball, respectively.

SEM observations were conducted on the wear tracks of both the plates and the balls for each pair of materials (displayed on Figure 3). These observations highlight strong differences in the wear tracks' morphology. First, the width of the tracks is not constant according to the insert displayed on the upper left of each SEM image of the BMG plate. The wear tracks of the brass ball/CuZr plate couple are about six times thinner than the others for both the plate and the ball. Secondly, the distribution and morphology of third bodies is different from one counterface to another. In addition, EDS analyses performed on each track allowed to identify the nature of third bodies and the potential eventual material transfer.

After rubbing against 440C, the CuZr plate is covered by homogeneously and evenly distributed patches making a quasi-continuous third body layer. The wear track of the 440C ball is covered by a continuous and rough third body layer and dark volatile particles that get trapped between patches at the extremities of the track. Third bodies of both the plate and the ball are composed of the oxidized elements of the CuZr plate (Zr, Cu and Al). A very small amount of Fe and almost no Cr is detected in the third body on the ball. Ejected particles remaining on the ball are also mainly composed of O, Zr, Cu and a low amount of C. An EDS analysis was also performed on the dark particles trapped along the patches (not displayed on Figure 3), that reveals a predominant presence of C (86 at%) mixed with small amounts of O, Cu and Zr.

After rubbing against 52100, the CuZr plate is covered by an inhomogeneous third body. The friction track is composed of both stripes deprived of third body and stripes rich in third body patches. The above-mentioned patches are large, smooth and seem to be formed by compacted wear particles. The 52100 ball has a perfectly circular wear scar without any apparent third body. Both the third body of the CuZr plate and the ejected particles are exclusively composed of Fe and O. On the 52100 ball, the compositions inside of the wear track and on the unworn surface are exactly the same, revealing the lack of material transfer.

After rubbing against brass, the track of the CuZr plate is extremely small in size and covered by very small patches (with a typical size inferior to 2 µm) distributed along straight lines parallel to the sliding direction. The wear track of the brass ball is covered by a thin layer of third body. The third body of the plate is composed of oxidized Zr, Cu and a surprisingly high amount of Zn (23 at%), which indicates material transfer from the brass ball to the CuZr plate. On the ball, the tribolayer on the wear scar is richer in Zn than the unworn surface, that might reflect a migration of Zn to the surface during friction. No Zr is detected on the ball, indicating that no, or very limited, material transfer from the BMG to the brass ball occurred.

After rubbing against bronze, small patches with a very regular shape are homogenously distributed all over the CuZr plate track. The wear track of the bronze ball is covered by a continuous and rough third body layer. The compositions of the third bodies and the ejected particles are very close to those of tests performed with 440C. This means that the third bodies of both the plate and the ball and ejected particles are composed of O, Zr, Cu and Al. Two findings suggest that the material transfer occurs from the CuZr plate to the bronze ball. First, no Sn is detected except on the pristine surface of the ball. Second, the Cu/Zr ratio is very close to the BMG composition, instead of exhibiting large Cu content.

After rubbing against both the Zr roller and the CuZr roller, two morphologies of third body patches are observed. With both counterfaces, the shape of patches is either large and thick or small and flat. However, the wear track of the counterpart is not similar between the Zr and CuZr rollers. On the one hand, the wear track of the CuZr roller is covered by a few lengthwise patches and many small dark dots. On the other hand, the wear track of the Zr roller is covered by several rough patches. The compositions of the third bodies of both the plate and the rollers and of the ejected particles are very close to those of tests performed with 440C and bronze. The Cu/Zr ratio of the third bodies is closer to the Cu/Zr ratio of the CuZr composition (richer in Cu) than the Zr composition (richer in Zr). This suggests that third bodies are more likely originating from the CuZr plate than from the rollers. Several

EDS spectra were also performed on the dark dots that are homogenously distributed over the entire wear track of the CuZr roller (not shown on Figure 3). Interestingly, they reveal a significant presence of C (65 at%) mixed with Cu, Zr and O.

4 Discussion

This study highlights a strong correlation between friction and wear resistance of $Cu_{45}Zr_{46}Al_7Nb_2$ and a phenomenon of material transfer with the countermaterial, that is related to the adhesive behavior of native oxides present on the surfaces before friction. Because of the thin thickness of native oxide compared to the wear volumes involved at the macroscopic scale, the role of native oxide was rather studied at the atomic and nm-scales. Caron *et al* [23], Kang *et al* [24] and Louzguine-Luzgin *et al* [25] all demonstrated that the wear resistance was increased and the friction coefficient lowered due to the presence of native oxide layers, after performing scratch tests using Atomic Force Microscopy (AFM) on $Ni_{62}Nb_{38}$, $Zr_{60}Cu_{30}Al_{10}$, and $Cu_{47}Zr_{45}Al_8$ metallic glasses, respectively. They also found that artificially grown surface oxide layer was responsible for an even higher wear resistance by increasing the oxide thickness up to 8-10 nm. At the macro-scale, the role of native oxide layers present on amorphous alloys during friction tests has been however first highlighted by Miyoshi and Buckley in 1986 [26]. They emphasized the ability of three Fe-based thin ribbons of metallic glass (MG) to provide a protective oxide film against wear in air, compared to 304 and 440C stainless steels that experienced higher wear under the same friction conditions. More recently, Prakash *et al* [16] performed a tribological study between several Fe-, Co-, and Ni-based MG rubbing against 52100 steel annular rings under reciprocating sliding motion. In their study, the material transfer occurs either from the steel counterface to the metallic glass (in case of Fe-based MG), or from the MG to the steel counterface (in case of Ni-based MG), providing an enhanced wear resistance of the surface protected by an oxide film. The nature of material transfer seemed to depend on the chemical composition of the MG as well as the countermaterial. They assumed that the formation of oxide layers is due to the high chemical reactivity of both surfaces and that the subsequent material transfer might be attributed to the chemical affinity of the oxides.

In the present study, three categories of tribological behavior of $Cu_{45}Zr_{46}Al_7Nb_2$ are identified according to the rubbing counterface material. Surprisingly, these categorizes are not correlated with the class of countermaterials (*i.e.* steels, Cu-based alloys and BMGs) but rather with the nature of the transferred material. On the one hand, a third body layer composed of the oxidized elements of the BMG forms on both the plate and the counterface when rubbing against 440C, bronze, CuZr and Zr. This material transfer from the CuZr plate to the counterface is responsible for a higher wear resistance of the counterface as compared to the BMG plate. Moreover, the friction coefficient is close to 0.5 for these four pair of materials because the contacting surfaces are eventually covered by the same oxides after a varying running-in period. On the other hand, a transferred layer composed of the elements originating from the counterface is formed on the BMG plate when rubbing against brass and 52100. The transferred layer ensures a high wear resistance of the BMG plate with the two countermaterials. However, the friction coefficient and wear rate of the counterface depend on the nature of oxides constituting the third body. When rubbing against 52100 balls, the third body formed on the CuZr plate is mainly composed of iron oxides that are responsible for a friction coefficient close to 0.66 and a severe wear of the steel ball. To the contrary, when rubbing against brass balls, the coefficient of friction is as small as 0.2 and the wear rate of the ball is close to zero. All the above-mentioned transfer phenomena might be partially explained by the nature of oxides formed.

The differences in behavior observed between 440C and 52100 might be explained by the stronger presence of Cr in 440C (16 wt%) than in 52100 (1.4 wt%). In a previous study performed with 52100 balls against BMGs, the iron oxide constituting the third body was identified as Fe_2O_3 particles, that

adhered to the BMG surface and were subsequently compacted into dense patches [3]. When rubbing against 440C, a completely different wear mechanism takes place due to the probable presence of Cr oxides and Cr carbides. Indeed, Cr oxides and carbides are known to induce abrasive wear of the rubbing counterface [27]. It might be assumed that the abrasive Cr oxides and/or Cr carbides from the 440C ball play a role in the early stages of wear, by inducing abrasive scratches and particles detachment of the BMG surface. Then, the detached particles originating from the BMG (Zr and Cu oxides) gather into a third body layer that adhere to both the ball and the plate. The detached particles present around the ball scar also contain a very small amount of Cr because they might be originating from the third body layer (Zr and Cu oxides mainly).

The difference observed between the bronze and the brass counterfaces may be related to Sn and Zn. Additional X-rays photoelectron spectroscopy analyses (XPS) were performed on two wear tracks of the CuZr plate after friction tests against brass and bronze counterfaces, in order to identify the nature of oxides responsible for such an opposite behavior using very similar materials. XPS analyses were performed with an Al Kα monochromatic excitation source. Information about the chemical elements constituting the extreme surface, until an approximate depth of 2 nm, are thus provided. Spectrums are displayed on Figure 4. The nature of oxides related to the BMG composition are ZrO_2, Cu_2O, $Al(OH)_3$ and Al_2O_3 with both countermaterials. The ZrO_2 peak shapes are slightly different between brass and bronze counterfaces, this is most likely due to the amount of Zr rather than to the nature of oxide. Indeed, all other Zr oxides (Zr_2O, ZrO and Zr_2O_3) have a binding energy smaller than 182 eV [28]. The Sn3d signal when rubbing with bronze is very weak, which means that there is a very small amount of Sn oxide. The nature of oxide might be both SnO or SnO_2, which have very close theorical binding energies (485.8 – 494.2 and 486.3 – 494.7 eV, respectively [29,30]). SnO_2 is however more probable, according to the measured binding energies (486.0 – 494.9 eV). In case of brass, the Zn LMM binding energy show a high amount of Zn in the tribofilm. The Zn2p3 spectrum does not inform the nature of oxide because all bending energies are very similar, but the ZnLMM spectrum enables to differentiate the Zn binding energy from the ZnO one (in theory 494.3 eV and 499.0 eV, respectively [31]). The larger area of the ZnO peak means that after friction tests, Zn is mainly under an oxidized form. A similar behavior of ZnO-enrichment of the extreme surface has been observed by Kong *et al* [32]. They performed pin-on-disk sliding tests using copper pins covered by a nanocrystalline Cu-Zn 100μm-layer against carbon steel disks. A ZnO enrichment occurred in the tribo-surface film, which contributes to the reduction of the friction coefficient up to 0.2 and to the formation of a steady and enduring tribofilm. Three mechanisms associated to brass can explain the combination of low friction and low wear: 1) The CuZn38 brass used in the present study has a two-phase α and β microstructure. The harder β-phase and the tougher α-phase provide an optimal structure to improve wear resistance [32] ; 2) The selective migration of Zn atoms to the extreme surface might be explained by the plastic deformation induced by frictional stress. The deformation creates a large number of vacancies and dislocation cells, that is in favor of the enrichment of solute atoms through diffusion. The high content of Zn in the surface is subsequently oxidized to ZnO. ZnO particles can limit cracks propagation by filling the voids of the tribofilm, which can reduce wear ; 3) ZnO particles are also known to act as solid lubricant in the contact [33]. These mechanisms may explain the remarkable tribological behavior of brass against $Cu_{45}Zr_{46}Al_7Nb_2$. However, the friction coefficient in the present study is ranging from 0.14 to 0.32, which suggests that the friction and wear mechanisms are not systematically the same from one test to another, although wear remains very low. This might be due to the two-phase α-β microstructure of CuZn38 brass, that can induce two behaviors, depending on whether α or β grains are located into the real contact area. This assumption will be addressed in future works.

During friction between CuZr plate and CuZr or Zr rollers, the friction and wear behaviors are really close to each other. The wear rate of the CuZr plate is slightly higher when rubbing against Zr rollers than CuZr rollers. This may be explained by the higher content of Zr in the Zr-roller composition, that leads to a higher concentration of ZrO_2 on the roller surface. ZrO_2 particles are known to be abrasive [34], and may lead to a higher wear of the CuZr plate. The major role played by Zr- and Cu-oxides

during friction may be correlated with the presence of a native oxide layer on the surface of BMGs, particularly when the main components exhibit a high affinity with oxygen (Zr, Cu, Al) [23]. The nature of this oxide layer has been previously studied at the nm-scale. Louzguine-Luzgin *et al* [25,35] studied the atomic structure of the native oxide present on the surface of $Cu_{47}Zr_{45}Al_8$ under ambient conditions. They showed that the oxide layer (approx. 10 nm thick) was mainly composed of amorphous ZrO_2 and Al_2O_3 oxides, with homogenously embedded crystalline Cu_2O nanoparticles of 5-10 nm in size. The presence of crystalline domains in the oxide layer has also been reported by Kang *et al* [24] and Miyoshi and Buckley [26]. Miyoshi and Buckley described small nuclei or clusters of 4 nm in size, which could enhance clustering and crystallization in amorphous alloys during sliding as a result of plastic flow, even at low sliding velocities and negligible temperature rise. Crystallites of α-Fe_2O_3 with size up to 150 nm were observed in the wear track. All these previous studies highlighted a complex structure of the native oxide layer present on the BMG surface, that may have a major role in material transfer that seems to be the predominant wear mechanism of BMGs in the present study.

In addition to the role of the native oxide film, the wear track of the CuZr roller (Figure 3) is covered by small dark dots rich in C (65 at%), that can only originate from the environment. This indicates strong reactions between the surface of BMGs with ambient air during friction, and more specifically with carbonaceous compounds. This could be explained first by an adsorbed film of oxygen and carbon, as it was observed by Miyoshi and Buckley by XPS [26]. Second, the friction process promotes further reactions with gases present in ambient air, leading to the formation of C-rich small dots in the track. Argibay *et al* [36] showed that a diamond-like carbon (DLC) film was tribochemically formed on the surface of a nanocrystalline Pt-Au alloy. This amorphous carbon film with embedded Pt-Au nanoparticles forms in the presence of organic adsorbates in air, and is extremely favorable to lower friction coefficients and increased wear resistance. This is consistent with the slightly higher wear resistance of the CuZr plate after friction against the CuZr roller than against the Zr roller (Figure 2), when considered in conjunction with the presence and absence of C-rich dots in the track, respectively.
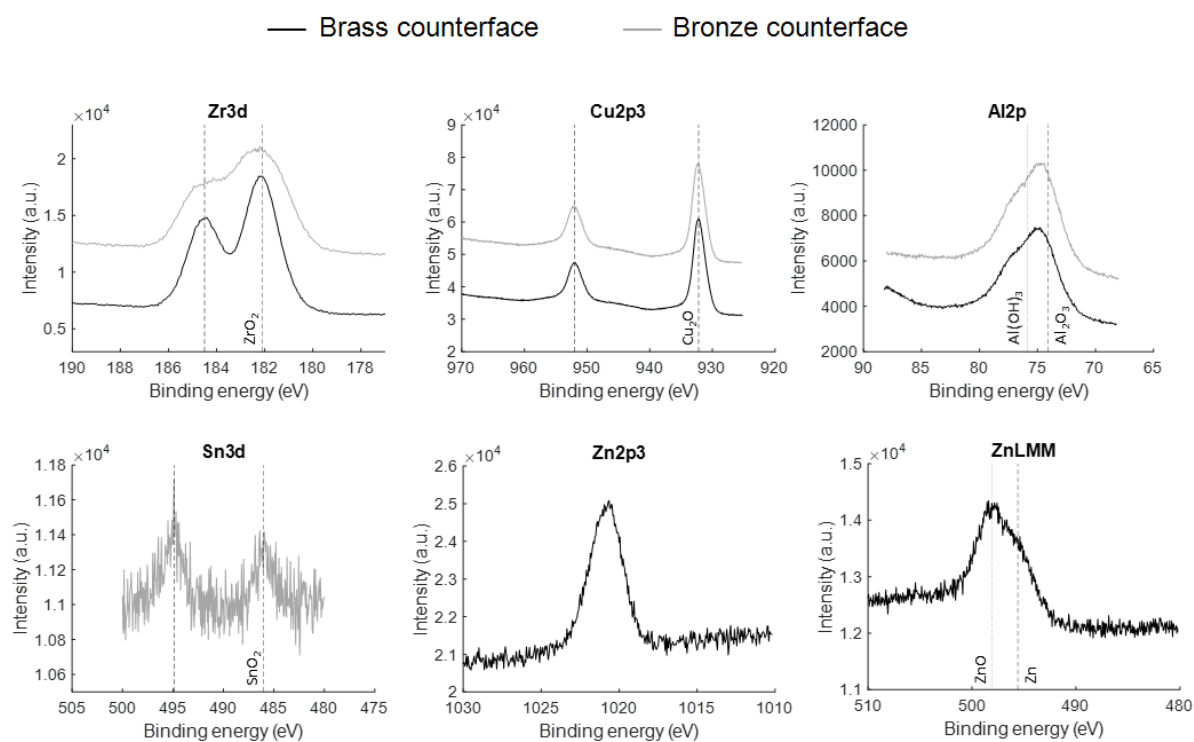

Figure 4 – XPS analyses conducted on the wear tracks of the CuZr plate after friction tests performed with brass and bronze balls, displayed by the black and grey curves, respectively.

5   Conclusion

The literature on BMGs seems to demonstrate that these specific materials do not follow the trend of higher wear resistance associated with higher hardness. The present paper confirms that the wear resistance of BMGs is not correlated with the hardness of the two materials in contact. Indeed, six countermaterials of different hardness were tested in sliding friction against a single BMG plate: two steels, two Copper-based alloys and two BMGs. The results show strong disparities in friction and wear depending on the countermaterial used. However, these disparities are not correlated with the hardness of the counterface, but with the chemical affinities and the formation of oxides in the contact interface: Fe_2O_3 and Cr oxides for steels, SnO_2 and ZnO for Cu-based alloys, ZrO_2 and Cu_2O for BMGs. Interactions between the oxides originating from the counterface and the oxides originating from the BMG plate are responsible for specific material transfer, that itself drives the level of friction and wear. Three categorizes of tribological behavior were established, depending on the counterface material:

- After rubbing against AISI 440C, bronze, and BMG counterfaces, material transfer occurred from the BMG plate to the counterface. This is responsible for a higher wear volume of the BMG plate, and a friction coefficient close to 0.5.
- After rubbing against the AISI 52100 counterface, material transfer occurred from the counterface to the BMG plate. This is responsible for a higher wear volume of the steel counterface, and a friction coefficient close to 0.7.
- After rubbing against the brass counterface, material transfer occurred from the counterface to the BMG plate. The large amount of ZnO in the third body might explain the remarkably low wear of both the plate and the counterface, as well as friction coefficient as low as 0.2.

6   Acknowledgements

7   References

[1]   J. Schroers, G. Kumar, T.M. Hodges, S. Chan, T.R. Kyriakides, Bulk metallic glasses for biomedical applications, JOM. 61 (2009) 21–29. https://doi.org/10.1007/s11837-009-0128-1.

[2]   M.M. Khan, A. Nemati, Z.U. Rahman, U.H. Shah, H. Asgar, W. Haider, Recent Advancements in Bulk Metallic Glasses and Their Applications: A Review, Critical Reviews in Solid State and Materials Sciences. 43 (2018) 233–268. https://doi.org/10.1080/10408436.2017.1358149.

[3]   S. Barlemont, P. Laffont, R. Daudin, A. Lenain, G. Colas, P.-H. Cornuault, Strong dependency of the tribological behavior of Cu-Zr based Bulk Metallic Glasses on relative humidity in ambient air, Friction. under review (n.d.). https://doi.org/10.1007/s40544-022-0680-z.

[4]   P.-H. Cornuault, G. Colas, A. Lenain, R. Daudin, S. Gravier, On the diversity of accommodation mechanisms in the tribology of Bulk Metallic Glasses, Tribology International. 141 (2020) 105957. https://doi.org/10.1016/j.triboint.2019.105957.

[5]   A. Caron, D.V. Louzguine-Luzguin, R. Bennewitz, Structure vs Chemistry: Friction and Wear of Pt-Based Metallic Surfaces, ACS Appl. Mater. Interfaces. 5 (2013) 11341–11347. https://doi.org/10.1021/am403564a.

[6] H. Zhong, J. Chen, L. Dai, Y. Yue, Z. Zhang, X. Zhang, M. Ma, R. Liu, Tribological behaviors of Zr-based bulk metallic glass versus Zr-based bulk metallic glass under relative heavy loads, Intermetallics. 65 (2015) 88–93. https://doi.org/10.1016/j.intermet.2015.06.002.

[7] B. Prakash, K. Hiratsuka, Sliding wear behaviour of some Fe-, Co- and Ni-based metallic glasses during rubbing against bearing steel, Tribology Letters. 8 (2000) 153–160. https://doi.org/10.1023/A:1019191303146.

[8] P.J. Blau, Friction and wear of a Zr-based amorphous metal alloy under dry and lubricated conditions, Wear. 250 (2001) 431–434. https://doi.org/10.1016/S0043-1648(01)00627-5.

[9] F. Jiang, J. Qu, G. Fan, W. Jiang, D. Qiao, M.W. Freels, P.K. Liaw, H. Choo, Tribological Studies of a Zr-Based Glass-Forming Alloy with Different States, Advanced Engineering Materials. 11 (2009) 925–931. https://doi.org/10.1002/adem.200900184.

[10] R. Salehan, H.R. Shahverdi, R. Miresmaeili, Effects of annealing on the tribological behavior of Zr60Cu10Al15Ni15 bulk metallic glass, Journal of Non-Crystalline Solids. 517 (2019) 127–136. https://doi.org/10.1016/j.jnoncrysol.2019.05.013.

[11] Z. Parlar, M. Bakkal, A.J. Shih, Sliding tribological characteristics of Zr-based bulk metallic glass, Intermetallics. 16 (2008) 34–41. https://doi.org/10.1016/j.intermet.2007.07.011.

[12] Y. Wang, L. Zhang, T. Wang, X.D. Hui, W. Chen, C.F. Feng, Effect of sliding velocity on the transition of wear mechanism in (Zr,Cu)95Al5 bulk metallic glass, Tribology International. 101 (2016) 141–151. https://doi.org/10.1016/j.triboint.2015.11.012.

[13] Q. Zhou, W. Han, D. Luo, Y. Du, J. Xie, X.-Z. Wang, Q. Zou, X. Zhao, H. Wang, B.D. Beake, Mechanical and tribological properties of Zr–Cu–Ni–Al bulk metallic glasses with dual-phase structure, Wear. 474–475 (2021) 203880. https://doi.org/10.1016/j.wear.2021.203880.

[14] E. Fleury, S.M. Lee, H.S. Ahn, W.T. Kim, D.H. Kim, Tribological properties of bulk metallic glasses, Materials Science and Engineering: A. 375–377 (2004) 276–279. https://doi.org/10.1016/j.msea.2003.10.065.

[15] H. Wu, I. Baker, Y. Liu, X. Wu, P.R. Munroe, J. Zhang, Tribological studies of a Zr-based bulk metallic glass, Intermetallics. 35 (2013) 25–32. https://doi.org/10.1016/j.intermet.2012.11.010.

[16] B. Prakash, Abrasive wear behaviour of Fe, Co and Ni based metallic glasses, Wear. 258 (2005) 217–224. https://doi.org/10.1016/j.wear.2004.09.010.

[17] Z. Liao, N. Hua, W. Chen, Y. Huang, T. Zhang, Correlations between the wear resistance and properties of bulk metallic glasses, Intermetallics. 93 (2018) 290–298. https://doi.org/10.1016/j.intermet.2017.10.008.

[18] K. Wu, L. Zheng, H. Zhang, Research on high-Al Cu-Zr-Al-Y bulk metallic glass and its composites, Journal of Alloys and Compounds. 770 (2019) 1029–1037. https://doi.org/10.1016/j.jallcom.2018.08.130.

[19] D.R. Maddala, R.J. Hebert, Sliding wear behavior of Fe50−xCr15Mo14C15B6Erx (x=0, 1, 2at%) bulk metallic glass, Wear. 294–295 (2012) 246–256. https://doi.org/10.1016/j.wear.2012.06.007.

[20] H.W. Jin, R. Ayer, J.Y. Koo, R. Raghavan, U. Ramamurty, Reciprocating wear mechanisms in a Zr-based bulk metallic glass, Journal of Materials Research. 22 (2007) 264–273. https://doi.org/10.1557/jmr.2007.0048.

[21] A. Aditya, H. Felix Wu, H. Arora, S. Mukherjee, Amorphous Metallic Alloys: Pathways for Enhanced Wear and Corrosion Resistance, JOM. 69 (2017) 2150–2155. https://doi.org/10.1007/s11837-017-2384-9.

[22] J.J. Ayerdi, A. Aginagalde, I. Llavori, J. Bonse, D. Spaltmann, A. Zabala, Ball-on-flat linear reciprocating tests: Critical assessment of wear volume determination methods and suggested improvements for ASTM D7755 standard, Wear. 470–471 (2021) 203620. https://doi.org/10.1016/j.wear.2021.203620.

[23] A. Caron, P. Sharma, A. Shluger, H.-J. Fecht, D.V. Louzguine-Luzguin, A. Inoue, Effect of surface oxidation on the nm-scale wear behavior of a metallic glass, Journal of Applied Physics. 109 (2011) 083515. https://doi.org/10.1063/1.3573778.

[24] S.J. Kang, K.T. Rittgen, S.G. Kwan, H.W. Park, R. Bennewitz, Importance of surface oxide for the tribology of a Zr-based metallic glass, Friction. 5 (2017) 115–122. https://doi.org/10.1007/s40544-017-0149-7.

[25] D.V. Louzguine-Luzgin, M. Ito, S.V. Ketov, A.S. Trifonov, J. Jiang, C.L. Chen, K. Nakajima, Exceptionally high nanoscale wear resistance of a Cu47Zr45Al8 metallic glass with native and

artificially grown oxide, Intermetallics. 93 (2018) 312–317. https://doi.org/10.1016/j.intermet.2017.10.011.

[26] K. Miyoshi, D.H. Buckley, Microstructure and surface chemistry of amorphous alloys important to their friction and wear behavior, Wear. 110 (1986) 295–313. https://doi.org/10.1016/0043-1648(86)90105-5.

[27] X. Cheng, Z. Jiang, D. Wei, H. Wu, L. Jiang, Adhesion, friction and wear analysis of a chromium oxide scale on a ferritic stainless steel, Wear. 426–427 (2019) 1212–1221. https://doi.org/10.1016/j.wear.2019.01.045.

[28] Z. Bastl, A.I. Senkevich, I. Spirovová, V. Vrtílková, Angle-resolved core-level spectroscopy of Zr1Nb alloy oxidation by oxygen, water and hydrogen peroxide, Surface and Interface Analysis. 34 (2002) 477–480. https://doi.org/10.1002/sia.1342.

[29] M.A. Stranick, A. Moskwa, SnO by XPS, Surface Science Spectra. 2 (1993) 45–49. https://doi.org/10.1116/1.1247723.

[30] M.A. Stranick, A. Moskwa, SnO2 by XPS, Surface Science Spectra. 2 (1993) 50. https://doi.org/10.1116/1.1247724.

[31] P. Lang, C. Nogues, Self-assembled alkanethiol monolayers on a Zn substrate: Interface studied by XPS, Surface Science. 602 (2008) 2137–2147. https://doi.org/10.1016/j.susc.2008.03.044.

[32] X.L. Kong, Y.B. Liu, L.J. Qiao, Dry sliding tribological behaviors of nanocrystalline Cu–Zn surface layer after annealing in air, Wear. 256 (2004) 747–753. https://doi.org/10.1016/S0043-1648(03)00528-3.

[33] F.A. Essa, Q. Zhang, X. Huang, A.M.M. Ibrahim, M.K.A. Ali, M.A.A. Abdelkareem, A. Elagouz, Improved Friction and Wear of M50 Steel Composites Incorporated with ZnO as a Solid Lubricant with Different Concentrations Under Different Loads, J. of Materi Eng and Perform. 26 (2017) 4855–4866. https://doi.org/10.1007/s11665-017-2958-2.

[34] J.K. Knapp, H. Nitta, Fine-particle slurry wear resistance of selected tungsten carbide thermal spray coatings, Tribology International. 30 (1997) 225–234. https://doi.org/10.1016/S0301-679X(96)00048-5.

[35] D.V. Louzguine-Luzgin, C.L. Chen, L.Y. Lin, Z.C. Wang, S.V. Ketov, M.J. Miyama, A.S. Trifonov, A.V. Lubenchenko, Y. Ikuhara, Bulk metallic glassy surface native oxide: Its atomic structure, growth rate and electrical properties, Acta Materialia. 97 (2015) 282–290. https://doi.org/10.1016/j.actamat.2015.06.039.

[36] N. Argibay, T.F. Babuska, J.F. Curry, M.T. Dugger, P. Lu, D.P. Adams, B.L. Nation, B.L. Doyle, M. Pham, A. Pimentel, C. Mowry, A.R. Hinkle, M. Chandross, In-situ tribochemical formation of self-lubricating diamond-like carbon films, Carbon. 138 (2018) 61–68. https://doi.org/10.1016/j.carbon.2018.06.006.